coatings

MDPI

Article

Modeling Wear of KNA-82 Coatings with 0.5% Yttrium for Radial Seals of Gas Turbine Engines

Vitaliy Kulikov [1], Vadim Kubich [2], Yelyzaveta Fasol [3], Oleg Cherneta [4], Svetlana Kvon [1], Aristotel Issagulov [1], Saniya Arinova [1] and Olga Zharkevich [5,*]

[1] Department of Metallurgy and New Materials, Faculty of Metallurgy and Mechanical Engineering, Abylkas Saginov Karaganda Technical University, Karaganda 100012, Kazakhstan; v.kulikov@ktu.edu.kz (V.K.); s.kvon@ktu.edu.kz (S.K.); a.isagulov@ktu.edu.kz (A.I.); s.arinova@ktu.edu.kz (S.A.)
[2] Department of Automobiles, Heat Engines, and Hybrid Power Plants, National University Zaporizhzhia Polytechnic, 69063 Zaporizhzhia, Ukraine; schmirung@gmail.com
[3] Department of Physical Materials Science, National University Zaporizhzhia Polytechnic, 69063 Zaporizhzhia, Ukraine; selvluna@gmail.com
[4] Department of Automobiles and Transport and Logistics Systems, Dniprovsk State Technical University, 51918 Kamianske, Ukraine; ocherneta@gmail.com
[5] Department of Technological Equipment, Faculty of Metallurgy and Mechanical Engineering, Abylkas Saginov Karaganda Technical University, Karaganda 100012, Kazakhstan
* Correspondence: zharkevich82@mail.ru; Tel.: +7-7017412664

Abstract

The paper presents the results of a study of linear wear of gas-flame and ion-plasma coatings of KNA-82 seals with an yttrium content of 0.5%, used in gas turbine engine assemblies, during physical modeling of their thermomechanical loading on small-sized samples. Tribotechnical tests were carried out in four stages, simulating the operating conditions of real gas turbine engines—from the first start-up with running-in of the coating cut-in areas to reaching a steady state with their service properties formed. The surface of the coatings was in contact with the ridges of triangular-shaped plates without heating (20 °C), at average heating (350–470 °C), after holding the samples at 1100 °C and average heating of 410–460 °C, and after grinding off the worn layer that had worn out after holding the samples at 1100 °C at average heating of 320–440 °C. Trends in the change in the linear ear of coatings and the formation of friction tracks caused by the uneven manifestation of the physical and mechanical properties of coatings, which are unevenly distributed throughout their body, were determined. It was found that both coatings tend to stabilize the wear process at certain mechanical pressures in the friction contact zone and only in the temperature range from 20 °C to 400 °C. These pressures range from 4 MPa to 6.7 MPa for gas-flame coatings and from 3 MPa to 4.2 MPa for ion-plasma coatings. It has been determined that within the depth range of 30–100 μm, the wear resistance (as assessed by linear wear) of ion-plasma coatings is higher than that of gas-flame coatings. This predetermines the fact that in the event of a catastrophic collision between the coatings and a blade, the geometry of the damage to the surface of the gas-flame coating will be greater than that of the ion-plasma coating. In the event of damage exceeding 75–100 μm in depth, both coatings become inoperable, since their wear characteristics are no longer maintained. This is indicated by a rapid decrease in their wear resistance under step loading. Moreover, the gas-flame coating is more prone to catastrophic failure than the ion-plasma coating.

Keywords: gas-flame coating; ion-plasma coating; yttrium; reduced linear wear; thermo-mechanical loading; wear track; temperature

Academic Editors: Vasileios Koutsos and Lech Pawlowski

Received: 17 January 2026
Revised: 16 February 2026
Accepted: 17 February 2026
Published: 20 February 2026

1. Introduction

Heat-resistant seal coatings are widely used in modern aircraft engine manufacturing [1]. Heat-resistant sealing coatings are composites applied to gas turbine engine stator elements (Figure 1) to create minimal radial clearances.

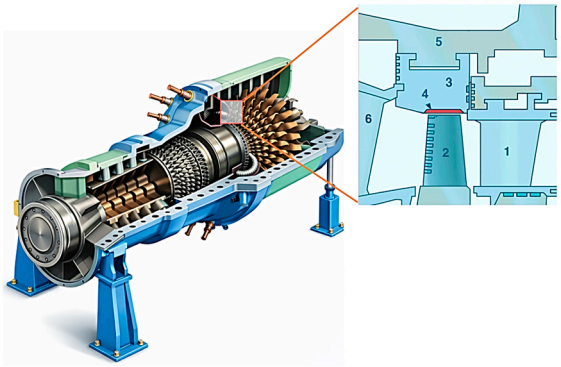

Figure 1. Location of the sealing coating in the gas turbine engine compartment: 1—first-stage guide apparatus; 2—first-stage turbine blade; 3—sealing band segment; 4—high-temperature ceramic sealing coating; 5—housing; 6—second-stage guide vane.

Their operation is based on the principle of controlled wear:

- Upon initial contact with the rotor, the coating wears away, minimizing gas leaks and increasing efficiency.
- As a result of temperature effects, secondary structures are formed, ensuring wear resistance and maintaining efficiency during service [1–3].

The current trend towards higher operating temperatures is aimed at increasing thrust and efficiency: for example, a 50 °C increase in combustion chamber temperature can increase efficiency by 12.5% [2–6]. Under these conditions, maintaining the functional properties of seals under extreme heat becomes critical for engine reliability.

Traditional sealing coatings of the KNA-82 system (7%–13% BN; 1.5%–2.5% C; 0.3%–1.2% Al; 1.4%–2.5% Si; the rest Ni) retain their performance up to temperatures of 900–950 °C, but modern and promising engines require materials capable of functioning reliably at temperatures of 1100–1200 °C [7]. Alloying coatings with rare earth metals, in particular, yttrium, is one of the most effective ways to increase their high-temperature resistance. The presence of these elements in the coating contributes to the formation of stable protective oxide films that increase resistance to gas corrosion and erosion wear [8–11].

Yttrium in appropriate proportions stabilizes aluminum and chromium oxide films, improves the adhesion of applied coatings to the substrate material, increases the thermal stability of alloys, and slows down the coagulation of strengthening phases. It has been established that yttrium dissolved in a nickel matrix increases heat resistance. The introduction of yttrium in an amount exceeding its solubility limit (for nickel, this is 0.2–0.3 wt. %) leads to the formation of a compound inside and at the boundaries of the grains, which is chemically similar to the Ni_3Y phase. The introduction of yttrium also promotes the formation of Ni (Cr, Al, Y)$_2O_4$ and (Cr, Y)$_2O_3$ oxides on the surface of the alloy. In Ni-Co-Cr-Al-Y coatings, Y segregation at the scale–coating interface leads to less cavity formation and, therefore, improves the adhesion of the α-Al_2O_3 oxide scale. The addition of yttrium in amounts of 0.1 and 0.4% improves the properties; however, a lower yttrium content of 0.1% gives a better result because there is less internal oxidation and, consequently, the onset of scale spalling is delayed for a longer period of time [12–17].

The most significant and currently used in production is the gas-flame and ion-plasma method of forming such coatings from finely dispersed powder of the appropriate compo-

sition [18–21]. Thus, in work [22], based on the results of tribotechnical tests of coatings from the KNA-82 system with the addition of 0.1%, 0.3%, and 0.5% yttrium, data were obtained that made it possible to establish the nature of changes in the dynamic friction coefficient during the test period and the values of the energy intensity of wear. The tests were simulated on small-sized samples using a "rotating disc–stationary block" scheme. The evaluation of coatings formed by gas-flame and ion-plasma methods was based on the fact that maximum resistance to mechanical destruction is determined by the manifestation of a constant minimum value of the dynamic friction coefficient as a sign of lower friction force before reaching the fatigue limit, and the number of separated particles that make up a unit of integral friction work. These evaluation parameters are ranked from one to four points. The maximum score corresponds to maximum resistance, i.e., a lower value of material wear energy capacity and a minimum value of the stable friction coefficient. It has been established that the same coincidence of these parameters according to the measurement results is observed at almost all stages of testing for a coating formed by the gas-flame method with an yttrium concentration of 0.3%–0.5%. The exception was the coating formed by the ion-plasma method with an yttrium concentration of 0.1% at the fourth stage of testing, i.e., after repeated high-temperature loading.

Study [23] showed that the KNA-82 gas-flame coating (0.1% Y) is more effective than the ion-plasma coating at high temperatures (350–800 °C), where its wear is two times lower. At low temperatures (up to 200 °C), it performs worse, and at 1100 °C, the properties of the coatings become identical. At the same time, ion-plasma coating is prone to thermal destruction of the structure.

The following are results of studies of KNA-82 coatings with yttrium. In works [24–26], based on the methods of [23], the following patterns were established: at 1100 °C, the ion-plasma coating exceeds the gas-flame coating in wear resistance by 10% (constant load) and 34% (step load). At the same time, the gas-flame coating maintains a stable wear mechanism in the range of 350 °C–1100 °C, while the ion-plasma coating exhibits instability when modes are changed. For compositions with 0.1%–0.5% yttrium, it was found that under static load (1100 °C), the mass increase in the samples grows linearly with increasing yttrium content. However, the nature of this increase under static conditions differs significantly from the indicators under dynamic load in a burning gas environment (950 °C–1020 °C).

The use of yttrium as an alloying additive in KNA-82 heat-resistant coatings is limited to a threshold of 0.5 wt.%, since exceeding this concentration triggers material degradation mechanisms that neutralize its positive effect. According to a preliminary study of the problem, in particular by the authors of [27], it is indicated that at high concentrations, yttrium forms brittle intermetallic (Ni_5Y) and yttrium-rich phases at grain boundaries, which have a low melting point and a tendency to oxidize. This forms "loose" oxides inside the coating, disrupting its integrity. Studies of Ni-Al-Y systems, which include KNA-82, show that an excess of Y at grain boundaries forms a brittle network that reduces plasticity and causes premature cracking during thermal cycling. The technical specifications for these alloys often limit the content of rare earth metals to 0.5% in order to maintain a balance between heat resistance and mechanical strength [28].

The results of studies of yttrium-containing coatings based on KNA-82 indicate a comprehensive approach to assessing the effectiveness of their performance properties for a corresponding set of tribotechnical parameters in physical modeling of thermomechanical loading. The missing link in the studies conducted exclusively on the tribological aspect is the establishment of the patterns of linear wear of the coating with 0.5% yttrium content in the KNA-82 composition according to the "fixed-ring–movable plates with triangular combs" scheme in a closed simulation chamber in accordance with the previously proposed

physical simulation methodology. The materials science component of these studies is undoubtedly the basis for revealing the predicted structural and phase transformations in the initial structures and is not considered in this article.

The purpose of the work is to establish the patterns of linear wear of KNA system coatings with an yttrium content of 0.5% in the initial composition, formed by gas-flame and ion-plasma methods on model rings in contact with movable plates with triangular ridges when simulating thermomechanical loading in a test chamber.

2. Materials and Methods

2.1. Materials

For tribotechnical testing, KNA-82 coatings (nickel base, silicon, aluminum, and solid lubricants (graphite and boron nitride) (ANEP-Metal, Zaporizhzhia, Ukraine) were used, which were formed on the inner side of small-sized ring samples with a thickness of 5 mm using gas-flame and ion-plasma methods. The rings were made of nickel alloy EI435 (KH78T) GOST 5632-2014.

To prepare the mechanical mixture for plasma spraying, nickel, silicon, and graphite powders were sieved through appropriate sieves, and urea powder was sieved through a 1.0 sieve. The components were then mechanically mixed in the appropriate proportions by weight: 97.5%–98.0% nickel, 2.0%–2.5% silicon, and 10% urea based on a 100% mixture. This mixing was carried out in a special mixer with an eccentric axis of rotation for 8 h with the addition of "bugs" in an amount of 30% of the total mass of the components. Yttrium, which had been previously ground, was added separately to the mixture.

After that, the mixture was annealed in an atmosphere of dissociated ammonia at a temperature of 950 °C for 4–4.5 h. The annealed mixture should have had a uniform gray color in the form of a briquette. After grinding and sieving through a 010 sieve, boron nitride (12%), graphite (2%), and aluminum (1%) were added to the ground mixture (85%).

The particle size of the powders used to form the coatings, after grinding and sieving through a 010 sieve, was no more than 100 μm. The particle size of the added powders (boron nitride, graphite, and aluminum) was presumably similar—up to 100 μm—since they were mixed with a base mixture of the same particle size distribution. A "1.0 mm sieve" refers to a laboratory sieve with a 1.0 mm square aperture; a "0.10 sieve" corresponds to 0.10 mm (100 μm). Applicable standards: EN ISO 4782:1987 (mesh screens) [29] and ISO 3310-1:2017 [30].

2.2. Surface Preparation and Coating Application Methods

To prepare the rod mixture for gas-flame spraying, mechanical mixing of the powder mixture with sodium silicate in specific proportions was used. The mixed materials were then extruded in the form of rods through a press with a die diameter of 4.5 mm and a length of 400–600 mm. The resulting rods were laid out on special sheets.

The surface of the part was prepared before applying the KNA-82 material by blasting it with electrocorundum of a specific grain size, air pressure, nozzle diameter, and blasting distance. After that, the part was cleaned of dust with compressed air. The sample of the base material was pre-degreased in a digestive bath.

For research purposes, coatings were formed using both methods: gas-flame and plasma—on the inner side of a ring 50 mm wide and 160 mm in diameter made of nickel alloy EI435 (KhN78T). The thickness of the applied coatings was the same and amounted to 5 mm for both types. Gas-flame spraying was performed using pre-prepared powder mixtures, which were mixed with liquid glass and pressed into rods with a diameter of 4.5 mm and a length of up to 600 mm. Before application, the surface was cleaned and treated with electrocorundum. The spraying process was carried out at acetylene pressures

of 0.8–1.2 atm, oxygen pressures of 4.0–5.0 atm, and air supply pressures of 4.0–5.5 atm; the distance from the nozzle to the surface was 80–100 mm, and the rod feed rate was 350–450 mm/min.

The plasma (ion-plasma) coating was applied using the ion PVD method using the same thoroughly mixed powder mixtures. Before coating application, the sample surface was degreased, after which plasma spraying was performed at a distance from the surface of 100–120 mm, a current of 400–450 A, a voltage of 40–50 V, an argon flow rate of 45 L/min (working), a nitrogen flow rate of 3–8 L/min, and a powder flow rate of 1.3–1.7 kg/h. The working gas pressure was 294 kPa, and the plasma torch travel speed was 10–30 mm/min. This process consisted of several stages. Air was evacuated from the chamber to prevent vapor particles from colliding with gas molecules. The target (the future coating material) was evaporated using an electron beam. Atoms of the evaporated substance converted into ions-charged particles. Plasma was formed. A negative potential was applied to the sample itself. Since the ions are positively charged, they rushed toward the sample at high speed. The ions were driven into the sample's surface, forming a dense and durable coating.

One sample was tested for each condition. The number of measurements in each of the areas considered was 14–16.

The thickness of the initially formed coatings on the ring samples is 5 mm, i.e., 5000 μm.

2.3. Equipment and Procedure for Conducting the Experiment

To simulate the thermomechanical loading of the coatings under study, the experimental equipment used in work [26] was employed. The elements of the test chamber and the coatings under study, which were performed on 2 ring sample, are shown in Figure 2. The equipment was installed on a test bench for testing Hiradastechniki Gepgyara U-808 series No. 326 automotive engine generator sets (Budapest, Hungary) with two modes of controlled drive shaft speed change.

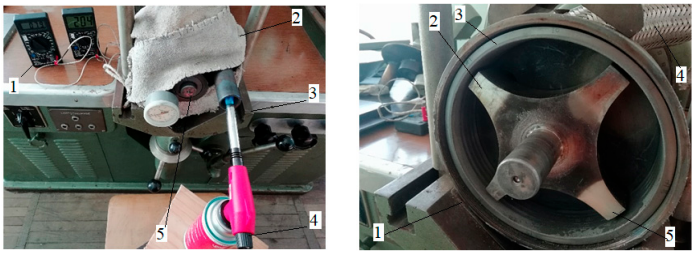

(**a**) (**b**)

Figure 2. Test setup: (**a**) top view; 1—multimeters; 2—test chamber insulation; 3—frame; 4—burner with isobutane–butane cylinder; 5—rotor shaft. (**b**) Test chamber without cover: 1—housing; 2—rotor; 3—ring sample; 4—outlet pipe; 5—cavity for placing plates.

Gas-flame spraying was performed using pre-prepared powder mixtures, which were mixed with liquid glass and pressed into rods with a diameter of 4.5 mm and a length of up to 600 mm. Before application, the surface was cleaned and treated with electrocorundum. The spraying process was carried out at acetylene pressures of 0.8–1.2 atm, oxygen pressures of 4.0–5.0 atm, and air supply pressures of 4.0–5.5 atm; the distance from the nozzle to the surface was 80–100 mm, and the rod feed rate was 350–450 mm/min.

Ion-plasma coating was performed using the same powder mixtures, which were thoroughly mixed. Before application, the surface was degreased, after which plasma spraying was carried out at a distance of 100–120 mm from the surface, with a current of 400–450 A, a voltage of 40–50 V, an argon flow rate of 45 L/min (working), a nitrogen flow rate of 3–8 L/min, and a powder flow rate of 1.3–1.7 kg/h. The working gas pressure was 294 kPa, and the plasma torch movement speed was 10–30 mm/min.

There were no deviations from the configuration of the experimental setup specified in [26]. The sequence of operations during the experiments was as follows. The coated ring sample 3 was installed in the housing after unscrewing the front cover, as seen in Figure 2. Then, the ring was secured with screws. Plates with triangular combs were placed in the grooves of rotor 2 (Figure 2b), as seen in Figure 3. Next, the front cover was installed by screwing it into the housing. The camera housing was secured with a mounting screw. The thermocouple wire splices were placed in the holes in the front cover and connected to the multimeters, Figure 2a. At the same time, the initial temperature was recorded. After that, the test chamber housing was thermally insulated using asbestos cloth (Figure 2a). Next, a gas cylinder and a gas burner (Figure 2a) were installed near the inlet of the test chamber. After that, the hot gas exhaust system was connected to the chamber from the rear of the housing (Figure 2b). The flow of burning gases created by igniting isobutane–butane with a piezoelectric element was directed into the inner cavity of the test chamber. Next, the rotor shaft drive was turned on (Figure 2a), and the required rotation speed was set. The temperature in the chamber cavities was monitored at the inlet and outlet. The data was recorded in the internal volume heating log. Without extinguishing the gas combustion flame, the temperature and nature of the thermomechanical interaction of the rotor teeth with the ring coating were monitored for acoustic effects throughout the test. The nature of the interaction is determined by the noise effects caused by the interaction of the plate ridges with the inner surface of the rings. The test time was set according to the conditions of the experimental stages. At the end of the experiment, the rotor drive was turned off, and the final temperature was recorded. Then, the flame was extinguished and the gas cylinder was removed to a safe place. The test chamber was then allowed to cool, the thermal insulation was removed, and the thermocouples were disconnected. After that, the test chamber was disassembled and the ring was removed. The wear tracks were micrometered. The resulting data array was then processed.

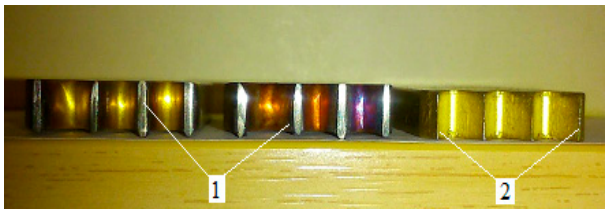

(**a**)

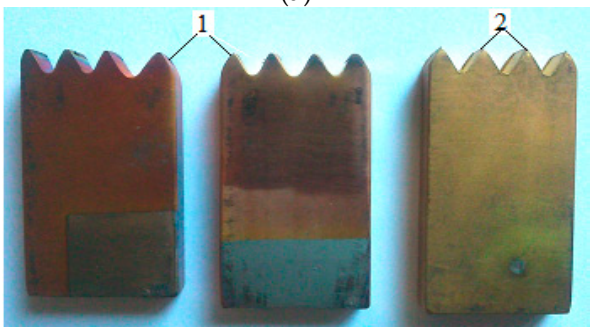

(**b**)

Figure 3. Plates: (**a**) view of the ends of the edges; (**b**) front view; 1—working edges (after testing); 2—original edges.

Chemical composition of the substrate made of alloy EI435 (KH78T): Ni 72%–78%, Cr 19%–22%, Ti 2.4%–2.8%, Fe up to 5%, Al up to 0.2%, Si up to 0.8%, Mn up to 0.5%, Cu up to 0.07%, C up to 0.1%, S up to 0.007%, and P up to 0.015%.

The plates were made of nickel alloy EI435 (KH78T) GOST 5632-2014 [31], and the ends of the ridges were coated with titanium nitride to increase wear resistance (Figure 3).

2.4. Wear Measurement

The method for measuring linear wear is shown in Figure 4. The following characteristics were used to assess wear:

- Linear wear h, which was converted to reduced wear h_{1000} to a friction distance of 1000 m. The need for such a conversion was determined by the change in the rotor speed (Figure 2a) when changing the modes of mechanical loading of the coating surface and different test durations.
- Conditional linear wear hy = h_{1000}/p_{av}, where p_{av} is the average pressure in the friction zone $p_{av} = 0.5(p_{min} + p_{max})$. The need to introduce this parameter was determined by the change in specific pressure in the friction zone. The minimum p_{min} and maximum p_{max} values of mechanical pressures were determined in accordance with the areas of the ends of plates, which increased during the test at the end of the experiment.

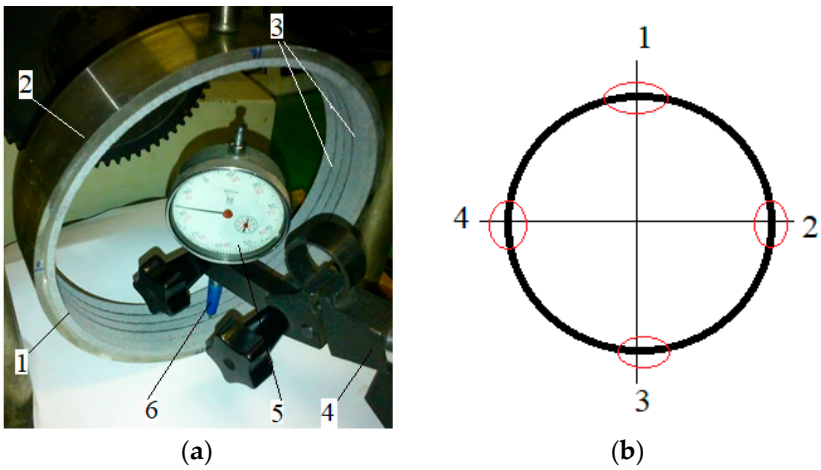

(**a**) (**b**)

Figure 4. Measurement of linear wear: (**a**) general view; 1—sample ring body; 2—coating; 3—wear tracks; 4—stand; 5—indicator head; 6—probe; (**b**) measurement areas (red circles): 1 – 0 degrees; 2 – 90 degrees; 3 – 180 degrees; 4 – 270 degrees.

The surface roughness was Ra = 2.5–6.3 μm.

When modeling the thermomechanical loading of the coatings under study, four possible stages of their contact interaction with the gas turbine blades were reproduced separately, spread out over time, and predicted to be characteristic of their operating conditions [32]. In this case, mechanical loading was simulated as constant and stepwise with possible levels determined by the contact areas in the friction zone and the contact force. Based on the technical capabilities of the stand on which the test chamber was mounted, as well as the mass and geometric parameters of the pressure plates (Figure 2b), the modes of force and speed loading of the friction contact zones were determined, which are given below for each of the stages.

3. Results

3.1. Results of Coating Testing at a Temperature of 20 °C (Stage 1)

Two experiments were conducted. Experiment No. 1 with constant loading and worn plate combs: test time t_t = 7 min, T = 20 °C, rotor speed n = 600 min^{-1}, pressure in the contact zone for gas-flame coating p_1 = 1.88–1.93 MPa, for ion-plasma coating p_2 = 1.83–1.88 MPa, and friction path L_t = 4167 m. Experiment No. 2 with constant loading with restored plate combs: test time t_t = 7 min, T = 21 °C, rotor speed n = 600 min^{-1}, pressure in the contact zone for gas-flame and ion-plasma coatings was p = 4.2 MPa, and friction path L_t = 4167 m.

The gas-flame coating worked smoothly with regular tapping of medium tone. The ion-plasma coating worked firmly with tapping that varied in character [33], from a soft, quiet knock to a harder, more resonant sound. Both coatings are gray in color. The structure of the gas-flame coating appears "loose," while that of the ion-plasma coating appears "dense." Visualization of the wear tracks formed on the coatings revealed the following (Figure 5). Based on experiment No. 1, the picture is as follows. Four wear tracks were formed at the points of interaction between the ends of the plate ridges and the coating surfaces. At the bottom of the wear tracks, there are scuffs with fragments of reinforced smoothing of irregularities, and the formation of shine on separate sections of the circumference, measuring 1.5–2.0 mm in length. Moreover, the density of such scuffing is lower for the gas-flame coating than for the ion-plasma coating. For the gas-flame coating, the outlines of the edges are less pronounced than for the ion-plasma coating. Based on experiment No. 2, the picture is as follows. Four wear tracks are also formed at the points of interaction between the ends of the plate ridges and the coating surfaces. For both coatings, there are continuous scuffs with a characteristic shine at the bottom of the wear tracks, characterized by smooth edges. While for the gas-flame coating, the bottom of the tracks in the horizontal plane is relatively flat in the gradient areas around the entire circumference, for the ion-plasma coating, there is undulation in these areas. These areas are characterized by lengths l1 = 5–10 mm of lesser depth, accounting for 60%–70% of the circumference, and lengths l2 = 10–15 mm of greater depth, accounting for 30%–40% of the circumference.

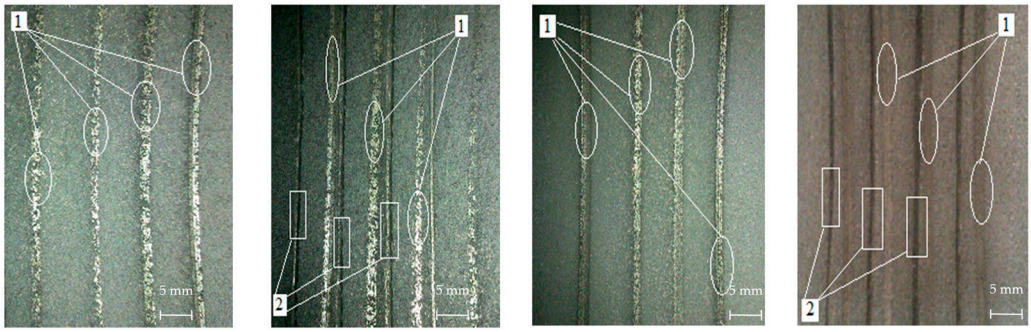

(**a**) (**b**) (**c**) (**d**)

Figure 5. Wear tracks on coatings: (**a**) on the surface of a gas-flame coating at p_1 = 1.88–1.93 MPa; (**b**) on the surface of a gas-flame coating. 1—marks after testing at p_1 = 1.88–1.93 MPa; 2—marks after testing at p_2 = 4.2 MPa; (**c**) on the surface of an ion-plasma coating at p_1 = 1.88–1.93 MPa; (**d**) on the surface of an ion-plasma coating: 1—marks after testing at p_1 = 1.83–1.88 MPa; 2—marks after testing at p_2 = 4.2 MPa.

3.2. Results of Coating Testing in the Temperature Range of 350–470 °C (Stage 2)

Two experiments were conducted. Experiment No. 1 under constant load: test time tt = 6 min, rotor speed n = 600 min^{-1}, pressure in the contact zone for gas-flame coating p1 = 2.14–11.3 MPa, for ion-plasma coating p_2 = 2.05–2.14 MPa, and friction path Lt = 3618 m. Experiment No. 2 with step loading: test time t_t = 0.51 + 22 + 0.53 = 3 min at rotor speeds n_1 = 600 min^{-1} and n_2 = 1200 min^{-1}, and friction path L_t = 3014 m. The pressures in the contact zone for the gas-flame coating were p_1 = 10 MPa, p_2 = 6.8 MPa, and p_3 = 1.13 MPa. The pressures were determined by calculation, taking into account the change in the average areas of the ends of the plate combs. For example, at a pressing force of F_1 = 14.43 N and S_1 = 1.44 mm^2, the pressure is p_1 = 10 MPa; at F_2 = 57.5 N and S_2 = 8.4 mm^2, the pressure is p_2 = 6.8 MPa; and at F_1 = 14.4 N and S_2 = 12.7 mm^2, the pressure is p_3 = 1.13 MPa. For the ion-plasma coating, the pressures were p_1 = 2.04 MPa, p_2 = 6.04 MPa, and p_3 = 1.18 MPa.

During experiment No. 1, the gas-flame coating worked stably, initially with very loud tapping (1–1.5 min), then more softly, but with dull rhythmic tapping. The ion-plasma coating worked stably with the same tone, softly with tapping.

During experiment No. 2, the gas-flame coating worked steadily with characteristic medium-pitched tapping. When switching from a rotation speed of 1200 min^{-1} to 600 min^{-1}, the sound became hoarse, i.e., it was associated with "wheezing." The ion-plasma coating also worked steadily with characteristic tapping sounds, but they were somewhat smoother and of a medium tone.

The results of experiment No. 1 are shown in Figure 6. The gas-flame coating had a gray surface color. Two extreme wear tracks were formed on the surface, while in the central part of the working surface, the wear tracks were barely visible. This is because the extreme ridges of the plates were made higher as a result of their restoration. The edges of the tracks are mostly even. The bottom of the tracks shows signs of moderate smoothing. At the same time, only in zone "3" over an arc length of 80 mm and in zone "0" over an arc length of 60 mm does the continuity of the bottom relief alternate between a dark matte color and a shiny steel color. The lengths of these sections are 7–8 mm for zone "3" and 3–5 mm for zone "0" for the dark matte color and 8–9 mm for the shiny steel color. Otherwise, the bottom of the tracks is silver-steel in color with traces of moderate smoothing. The surface structure is less dense than that of the ion-plasma coating.

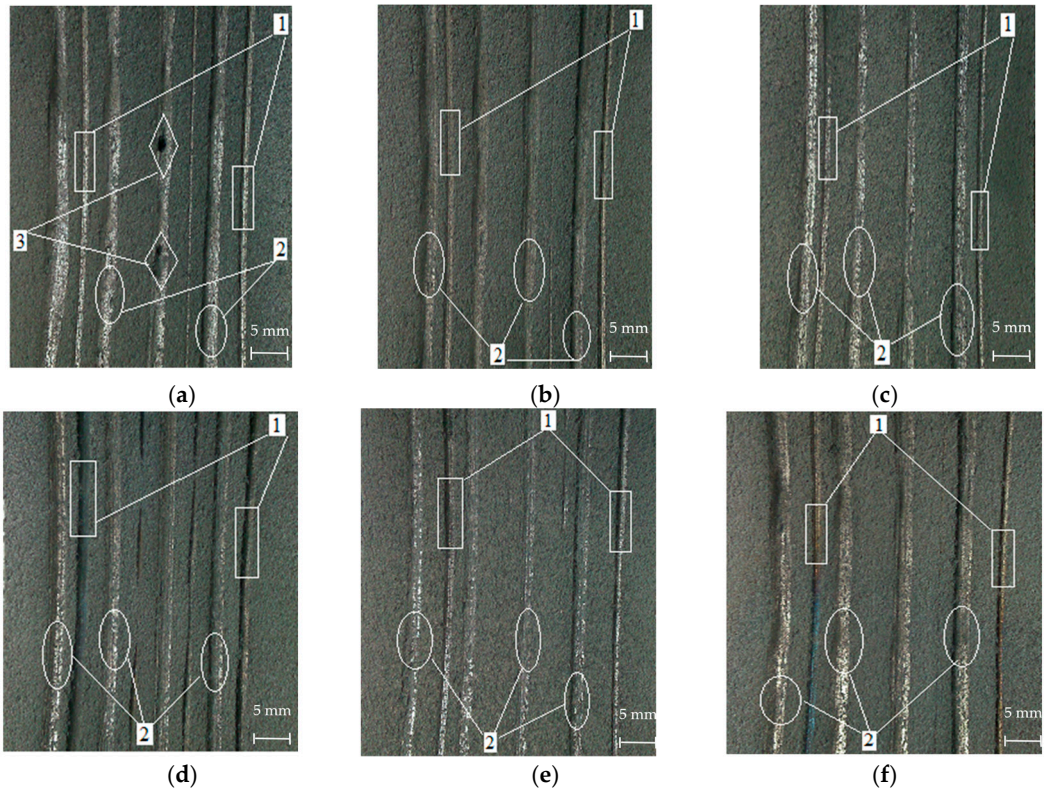

Figure 6. View of gas-flame coating surfaces after wear at stage No. 2: (**a**) zone "1", (**b**) zone "1-2"; (**c**) zone "2"; (**d**) zone "3"; (**e**) zone "0"; (**f**) zone "3-0". 1—experiment No. 1; 2—experiment No. 2; 3—pits.

The ion-plasma coating had a gray surface color. Two extreme wear tracks were formed on the surface, while in the central part of the working surface, the wear tracks were barely visible. This is due to the fact that the extreme ridges of the plates were made higher as a result of their restoration. The edges of the tracks are mostly even. The bottom of the tracks shows signs of moderate smoothing. However, only in zone "3" along an arc length of 80 mm does the continuity of the bottom relief alternate between a dark matte

color and a shiny steel color. The length of these sections is 5–6 mm. Otherwise, the bottom of the tracks is silver-steel in color with signs of moderate smoothing. The surface structure of the coating is dense.

The results of experiment No. 2 are shown in Figure 7.

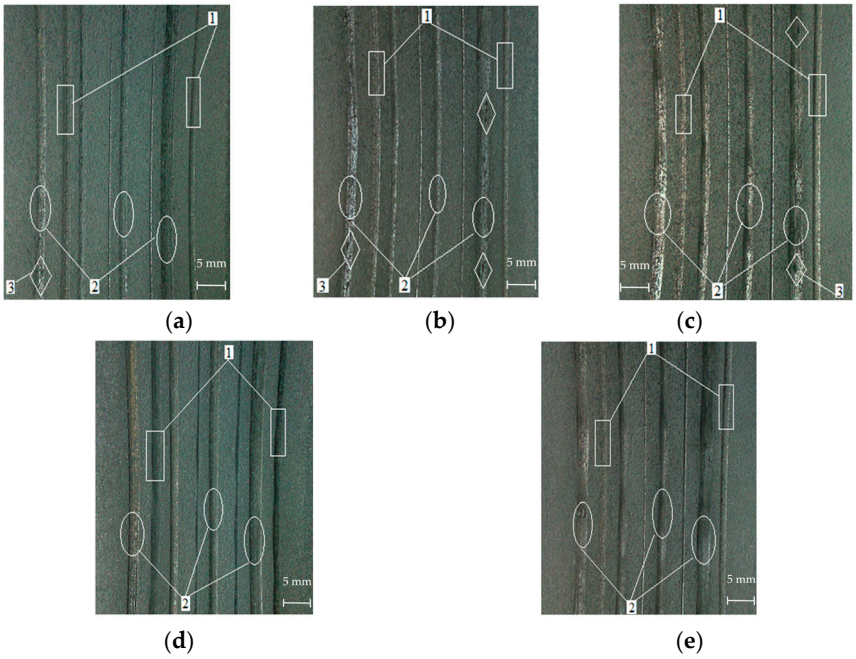

Figure 7. Appearance of ion-plasma coating surfaces after wear at stage No. 2: (**a**) zone "0"; (**b**) zone "1"; (**c**) zone "2"; (**d**) zone "3"; (**e**) zone "1-2". 1—experiment No. 1; 2—experiment No. 2; 3—pits.

The gas-flame coating had a gray surface color. Two extreme wear tracks were formed on the surface, while in the central part of the working surface, the wear tracks were less pronounced. This is because the extreme ridges of the plates had a greater height as a result of their wear in experiment No. 1. The edges of the tracks are mostly flat, but in some areas, they have a wavy contour. In measurement zone "1" on an arc 150 mm long, the contours are pulsed in nature with an amplitude increase to 0.5 mm in areas 6–9 mm long. In measurement zone "3-0," on a 50 mm arc, the contours are pulsed in nature with an increase in amplitude to 0.2 mm in sections 9–12 mm long. This may indicate heterogeneity in the distribution of material hardness within the near-surface layers at the depth of the observed wear. The bottom of the tracks shows traces of moderate smoothing alternating with traces of strip-like depressions in the relief, with a ratio of 40% to 60%. The continuity of the bottom relief has alternating matte and shiny shades. This indicates a clearly pronounced heterogeneity of the microgeometric parameters of the bottom surface roughness. Three shells are formed in measurement zone "2": one measuring 0.1 × 3 × 0.2 mm, the second measuring 4 × 1.5 × 0.2 mm, and the third measuring 2 × 2.5 × 2 mm. The surface structure is less dense than that of the ion-plasma coating.

The ion-plasma coating had a gray surface color. Two extreme wear tracks were formed on the surface, while in the central part of the working surface, the wear tracks were less pronounced. This is due to the fact that the extreme ridges of the plates had a greater height as a result of their wear in experiment No. 1. The edges of the tracks are mostly even, except for measurement zone "1-2" on a 75 mm long arc, which has a pulse-like outline with an amplitude increase of up to 0.2 mm on sections 6–8 mm long. The bottom of the tracks shows signs of moderate smoothing, but a fairly noticeable number of small shells ranging from 0.1 × 0.1 mm to 0.5 × 1.0 mm can be seen, which are mainly concentrated in measurement zone "1" on an arc of 130 mm, accounting for 2%–3% of the total. The relief

of the bottom in measurement zone "1-2" on an arc 100 mm long is pitted—alternating between smaller (section length 4–6 mm, dark color) and larger depths in sections 9–11 mm long, silver-steel in color. On the remaining surfaces, the bottom is silver-steel in color with traces of moderate smoothing and strip-like depressions in the relief. The surface structure of the coating is dense.

The parameters for assessing linear wear are given in Table 1.

Table 1. Summary data on the reduced h_{1000} and conditional h_y linear wear of coatings.

Coatings	Mode (Experience)	Parameter	Interaction Temperature			
			Stage 1 20 °C	**Stage 2 350–470 °C**	**Stage 3 1100 °C**	**Stage 4 1100 °C ***
Gas-flame coating	1	h_{1000}, μm	9.35 ± 2.6	30.4 ± 8.6 * 87.3 ± 9.4	-	-
		h_y, μm·MPa^{-1}	4.9	4.5 * 13.05	-	-
	2	h_{1000}, μm	54 ± 9.3	41.5 ± 8 * 69 ± 7	21.6 ± 7.6	66.7 ± 26.2 * 352 ± 33 * 227 ± 40
		h_y, μm·MPa^{-1}	12.9	6.9 * 11.5	5.8	12.35
Ion-plasma coating	1	h_{1000}, μm	11 ± 3.3	21.3 ± 6.4 * 35.6 ± 8.3	-	-
		h_y, μm·MPa^{-1}	5.9	10.1 * 16.9	-	-
	2	h_{1000}, μm	20 ± 6.5 * 47.8 ± 7.9 *	22.9 ± 7.3 * 43.5 ± 11	12.9 ± 4.9	21.3 ± 7.1
		h_y, μm·MPa^{-1}	4.76 * 11.4 *	7.4 * 14.12	2.18	6.6

Note. *—in a separate zone (areas*); *—after abrasive action.

For both coatings in stage 2 (experiment No. 1), there is an increase in the reduced linear wear compared to stage 1 (experiment No. 1). For the gas-flame coating, it is 3.2 times higher (9.3 times in a separate zone), and for the ion-plasma coating, it is 1.9 times higher (3.2 times in a separate zone). At the same time, the mechanical pressure for the gas-flame coating was 3.2 times lower than for the ion-plasma coating. This presumably indicates that under conditions of heating to a temperature of 350 °C–450 °C under constant loading, the intercomponent bonds in the material compositions are weakened. At the same time, this is more pronounced for the gas-flame coating than for the ion-plasma coating.

At stage 2 (experiment No. 1), within the limits of root mean square deviations, the linear wear of both coatings in relation to stage 1 (experiment No. 2) remained virtually unchanged, with the exception of certain areas. In these areas, only the gas-flame coating showed a 1.3-fold increase in wear, while the ion-plasma coating showed no change in wear within the standard deviations. This presumably indicates that stepwise loading predetermines the compaction of coating structures within the limits of possible elastic–plastic deformations in the tangential direction. At the same time, the effectiveness of micro-pressing processes of the thinnest surface layers is more pronounced in the gas-flame coating. This is indicated by the fact that its conditional linear wear decreased by 1.8 times in areas that exclude the formation of pits on friction tracks. For ion-plasma coatings, conditional wear increased by 1.2–1.5 times compared to stage 1 (experiment No. 2).

In general, it is noted that the resistance to mechanical stress in stage 2 (experiment No. 2) is higher for the gas-flame coating than for the ion-plasma coating. This is indicated

by the fact that the conditional wear of the gas-flame coating, taking into account constant and stepwise loading, is 1.4 times less than that of the ion-plasma coating. The ratio of conditional wear at stage 2 (experiment No. 1 and experiment No. 2) is 6.68 μm·MPa^{-1} for the gas-flame coating and 12.15 μm·MPa^{-1} for the ion-plasma coating.

3.3. Results of Coating Testing After Exposure to a Furnace at 1100 °C for 3 H (Stage 3)

One experiment was carried out under step loading: the test temperature was 410–460 °C, the test time t_t = 0.51 + 22 + 0.53 = 3 min, respectively, at the rotor speeds n_1 = 600 min^{-1} and n_2 = 1200 min^{-1}, and the friction path L_t = 3014 m.

A constant-load test was not conducted, as processing of the obtained wear tracks indicated minimal measurable linear wear when simulating high mechanical pressures and the coatings' presumably high resistance to damage. This means that to induce wear, it would have been necessary to either increase the test duration, which is difficult given the friction temperature regime, or increase the mechanical pressure, which is difficult given that no attention was paid to plate-end wear patterns.

The pressures in the contact zone for the gas-flame coating were p_1 = 2.12 MPa, p_2 = 7.6 MPa, and p_3 = 1.4 MPa. The pressures were determined by calculation, taking into account the change in the average statistical areas of the end faces of the plate combs. For example, with a pressing force of F_1 = 13.8 N and S_1 = 6.5 mm^2, p_1 = 2.12 MPa, with F_2 = 55.1 N and S_2 = 7.2 mm^2, p_2 = 7.6 MPa, and with F_1 = 13.8 N and S_3 = 9.6 mm^2, p^3 = 1.4 MPa. For the ion-plasma coating, the pressures were p_1 = 4.31 MPa, p_2 = 11.2 MPa, and p_3 = 2.1 MPa.

During the experiment, both coatings performed without jamming.

There was significant wear on the plate ends, but minor wear on the coating surface and particle separation in the form of very small flakes and peeling. These particles left no trace on the paper, meaning that they were "dry."

The flame coating operated quietly at a rotation speed of 600 min^{-1}, without the characteristic tapping sounds heard in stage 1. At 1200 min^{-1}, the rhythmicity intensified, and the tapping sounds were not noticeable. Upon switching to 600 min^{-1}, a hoarse, dull sound emerged, clearly reproducing the constant scraping of combs on the friction track surface.

The ion-plasma coating operated quietly, with light, rhythmic tapping sounds of uniform pitch. However, no obvious differences were heard at frequencies of 600 min^{-1} and 1200 min^{-1}.

The gas-flame coating had a surface color that was predominantly black with green inclusions, which formed as stripes 8–12 mm wide with distances between them from 0 mm to 15 mm, Figure 8. The density of the green background is variable. In measurement zone "2" on a 150 mm arc with a width from 10 mm to 25 mm and in zone "0" on arcs 20 mm long and 10–15 mm wide, and on an arc 65 mm long and 8 mm to 20 mm wide, the coating color is gray-green with a pearlescent tint. These signs indicate clearly pronounced heterogeneity of oxidation processes in the thinnest surface layers, caused by holding at a temperature of 1100 °C. The edges of the tracks are smooth and clearly defined. The bottom of the tracks has traces of high smoothing polishing. The color of the bottom is uniform dark gray. The surface structure of the bottom of the tracks is solid, appears to be of very-high density, and is far from loose.

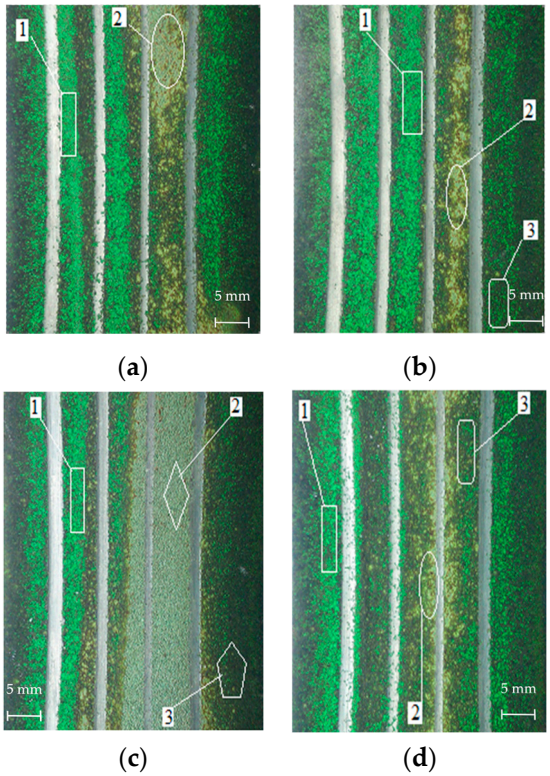

Figure 8. Wear tracks of the flame-sprayed coating: (**a**) zone "0"; (**b**) zone "1"; (**c**) zone "2"; (**d**) zone "3"; 1, 2, 3—characteristic areas with oxides.

The ion-plasma coating had a predominantly dark-green surface color with black inclusions randomly distributed in narrow stripes ranging from 4 mm to 10 mm in width and 10 mm to 70 mm in length (Figure 9). The density of the black background is variable. These features indicate mildly heterogeneous oxidation processes in the finest surface layers, caused by exposure to a temperature of 1100 °C. The track bottoms show traces of high-level smoothing and polishing. The bottom color is uniformly dark gray. The track bottom surface structure is largely continuous, apparently very dense, and far from loose. However, tiny fragments of porosity are visible on the bottom. This pattern of wear track formation resembles flat-top grinding of a porous surface. Moreover, this was evident in the ion-plasma coating at a lower wear depth compared to the gas-flame coating, on which such effects were not visible.

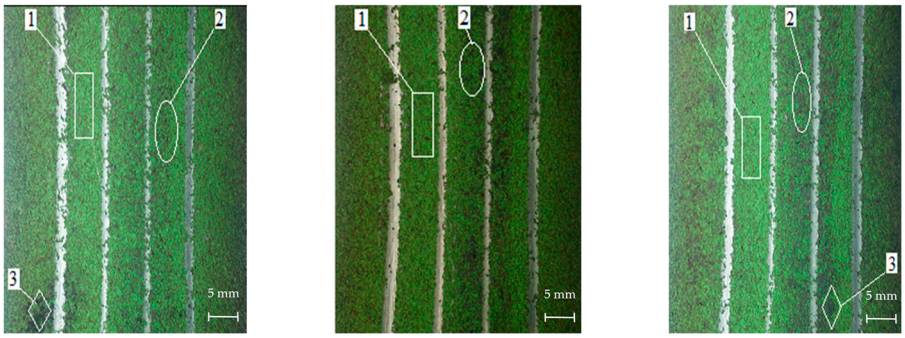

Figure 9. Wear tracks of the ion-plasma coating: (**a**) zone "0"; (**b**) zone "1"; (**c**) zone "2"; 1, 2, 3—characteristic areas with oxides.

For both coatings, there is a reduction in the reduced linear wear compared to stage 2 (experiment No. 2). For the gas-flame coating, it is 1.9 times lower, and for the ion-plasma

coating, it is 1.8 times lower. At the same time, the mechanical pressure for the gas-flame coating was 1.6 times lower, and for the ion-plasma coating, it was 1.9 times higher compared to stage 2 (experiment No. 2). This presumably indicates that when heated to a temperature of 400 °C–450 °C after aging at 1100 °C, the gas-flame coating is more prone to weakening of intercomponent bonds in its composition than the ion-plasma coating.

In general, it is noted that the ion-plasma coating has greater resistance to mechanical stress than the gas-flame coating. This is indicated by the conditional wear, which is on average 2.6 times greater for the gas-flame coating than for the ion-plasma coating.

3.4. Results of Testing Coatings on a Polished Worn Layer After Stage No. 3 (Stage 4)

One experiment was carried out under step loading: the test temperature was 320–440 °C, the test time t_t = 0.51 + 22 + 0.53 = 3 min, respectively, at the rotor speeds n_1 = 600 min^{-1} and n_2 = 1200 min^{-1}, and the friction path L_t = 915 m.

The contact zone pressures for the gas-flame coating were p_1 = 6.1 MPa, p_2 = 8.5 MPa, and p_3 = 1.6 MPa. The pressures were determined by calculation, taking into account the change in the average statistical areas of the plate comb ends. For example, with a pressing force of F_1 = 12.32N and S_1 = 2.03 mm^2, p_1 = 6.1 MPa, with F_2 = 49.3N and S_2 = 5.8 mm^2, p_2 = 8.5 MPa, and with F_1 = 12.32N and S_3 = 7.6 mm^2, p_3 = 1.6 MPa. For the ion-plasma coating, the pressures were p_1 = 1.6 MPa, p_2 = 6.7 MPa, and p_3 = 1.3 MPa.

Both coatings operated reliably throughout the experiment, with no jamming occurring. However, the flame coating created resistance to rotation during rotor start-up due to the small surfaces of the plate combs and their active cutting into the recessed layers of the material. This resulted in some jamming during start-up. A reliable start with sliding of the plates, loosely seated in the rotor, was achieved on the third attempt. The flame coating produced dull, rhythmic tapping sounds at a rotation speed of 600 min^{-1}. At 1200 min^{-1}, the tapping sounds became louder and remained rhythmic. The ion-plasma coating did not jam during start-up. The sound was much lower than that of the flame coating, and tapping sounds were practically inaudible. The sound at 600 min^{-1} was rustling, while at 1200 min^{-1} it was louder and rhythmic.

The flame-treated surface is matte gray. This may indicate the absence of oxidation spreading into the grinding depth. Four double wear tracks of variable width and depth are formed on the surface (Figure 10). The track edges are generally smooth and clearly defined. In zone "0," where the scallops are more deeply embedded, the track edges exhibit brittle chipping in places. The track bottoms show traces of moderate smoothing. The track bottoms are a uniform, matte–shiny dark gray. The track bottom surface structure is generally of moderate continuity, not loose. However, in zone "3," on an 80 mm long arc, on surface fragments with a more shiny, pearlescent hue, the track bottoms are black, polished, and continuous. In zone "1-2," the wear track bottoms are far from uniform, appearing jagged. The relief is a combination of thin, shiny stripes measuring 2 × 0.4 mm (possibly composed of the coating matrix metal–Ni, Cr) alternating with matte, loose depressions measuring 0.3 × 0.5 mm. These features indicate a pronounced heterogeneity in the mechanical properties of the sublayer formed after grinding off the previous layer. Overall, the coating surface structure outside the wear zones is continuous, appearing very dense, and not loose.

The surface of the ion-plasma coating is matte, gray-green in color, with variable density of distribution, both along the perimeter and along the visible surface relief. This may indicate the spread of oxidation processes into the grinding depth, albeit with some heterogeneity.

Grinding was performed to expose the surface and allow the plate profiles to cut into it. Grinding was performed to assess the wear of deeper layers in the event of destruction

of the formed surface structures at a depth of more than 50 µm. The latter is possible in the event of catastrophic cutting, which is not systematic in nature.

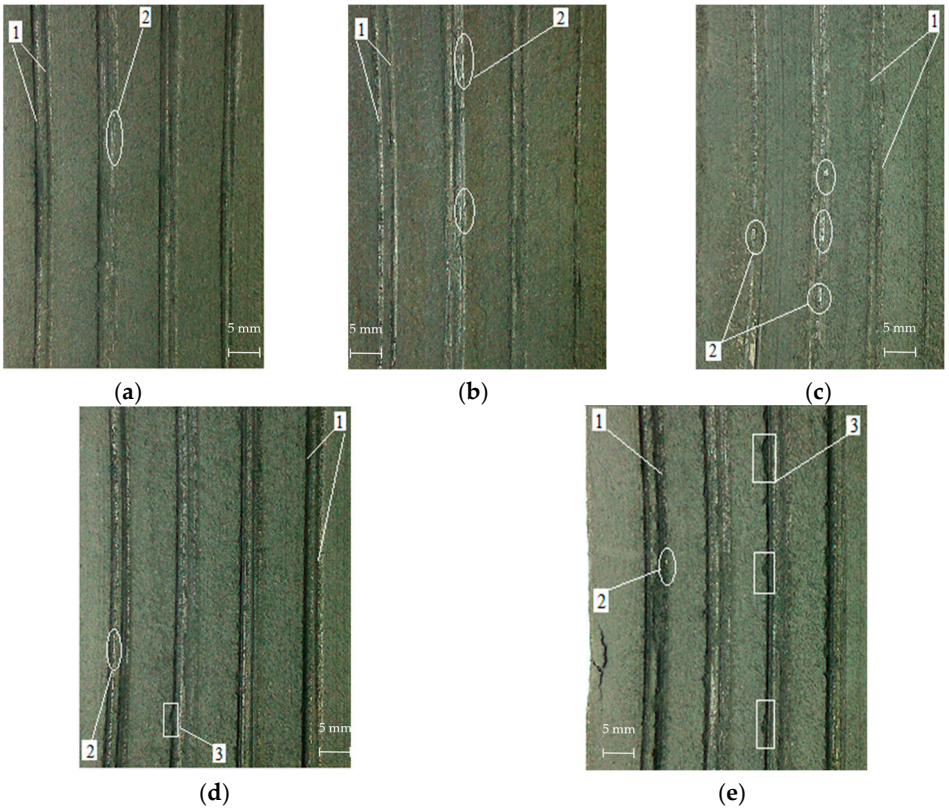

Figure 10. Flame-cut coating wear tracks: (**a**) zone "0"; (**b**) zone "1"; (**c**) zone "2"; (**d**) zone "3"; (**e**) zone "3-0". 1—double marks; 2—fragments of metal formations; 3—brittle chips.

Four wear tracks of approximately equal width and variable depth are formed on the surface (Figure 11). The track edges are generally smooth and clearly defined. No brittle chipping of the track edges is observed. The track bottoms generally show traces of high-level smoothing and polishing. The color of the track bottoms is generally matte dark and uniform. The surface structure of the track bottoms is generally highly continuous and not loose.

However, in zone "1-2" on an arc 70 mm long, a more complex relief has formed on the track bottoms. This relief consists of alternating rolled flakes of a shiny steel color of various flat geometric shapes (square, rectangle, elongated oval, and irregular triangle) ranging in size from 0.2 × 1.5 to 3 × 2 mm, seemingly superimposed on the bottom surface of the same matte black color. Moreover, their alternation is variable, with intervals from 1–1.5 mm to 10–15 mm (made of the coating matrix metal–Ni, Cr). In zone "2-3" on a 50 mm long arc along one of the tracks, the bottom relief is also clearly different. It is a loose structure with alternating shiny steel and matte black tones of variable density. The ratio of the shiny loose structure to the matte black is on average 15% to 85%. A similar bottom relief pattern formed on a 70 mm arc in zone "3-2" on one of the wear tracks. These features indicate pronounced heterogeneity of the mechanical properties of the sublayer formed after grinding off the previous layer. Overall, the coating surface structure outside the wear zones is of variable continuity, medium density, and appears loose.

For both coatings, the reduced linear wear increased compared to stage 3. For the flame coating, it was three times greater, while for the ion-plasma coating, it was 1.6 times greater. Furthermore, the mechanical pressure for the flame coating was 1.5 times greater, while for the ion-plasma coating, it was 1.8 times lower compared to stage 3. This presumably

indicates that wear due to plastic deformation occurs in the near-surface layers of both coatings, with similar intensity. Overall, the ion-plasma coating exhibits greater resistance to mechanical loading than the flame coating. This is indicated by the reduced wear, which is, on average, 1.9 times greater for the flame coating than for the ion-plasma coating.

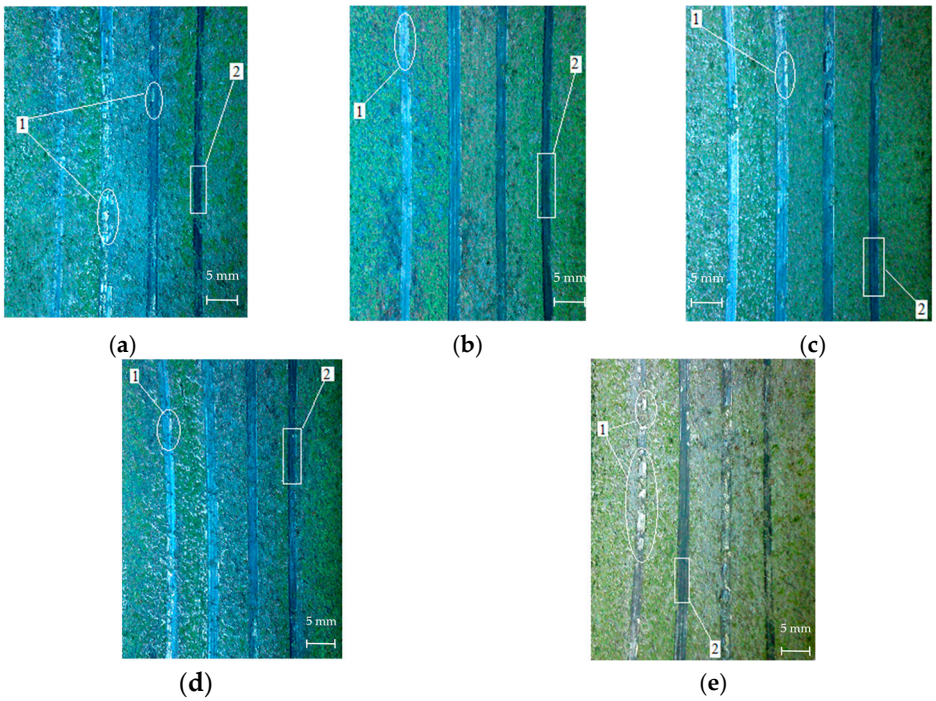

Figure 11. Wear tracks of the ion-plasma coating: (**a**) zone "0"; (**b**) zone "1"; (**c**) zone "2"; (**d**) zone "3"; (**e**) zone "3-2". 1—fragments of metal formations; 2—traces of polishing the bottom.

4. Discussion

Based on the data presented in Table 1, graphs (Figure 12) were constructed showing the predicted patterns of changes in the types of linear wear of the coatings depending on friction zone pressure and the temperature of the interface. The results shown in Figure 12 suggest the following.

First, the coating wear pattern varies across interface temperature ranges.

For example, in the temperature range from 20 °C to 400 °C, the reduced wear of both coatings remains virtually unchanged and constant with an increase in pressure on the flame coating from 4.2 MPa to 6.7 MPa (Figure 12a) and a decrease in pressure on the ion-plasma coating from 4.2 MPa to 3.1 MPa (Figure 12b). This indicates a steady-state wear process for flame coating No. 1. However, with an increase in the simulated pressure from lower values, from 1.9 MPa to 6.7 (3.1) MPa, a steady-state wear process is not observed. The reduced wear of the gas-flame coating increases at a higher rate than that of the ion-plasma coating, and this is explained by its higher interval pressure of 6.7 MPa. This picture can be explained by the following reasoning. High values of mechanical pressures (4.2 MPa → 6.7 MPa; 4.2 MPa → 3.1 MPa) in the friction zone [34], regardless of the temperature of the interaction medium, cause a decrease in the intrastructural distances between the coating components. At the same time, the forces of interaction between them increase. The stability of such bonds is higher for the gas-flame coating, since only for this coating does the reduced wear decrease with increasing pressure (Figure 12c). This demonstrates the manifestation of structural adaptability in the flame-exchanged coating to mechanical loading during compaction of its structure [35]. Resistance to overcoming the forces of interaction between the coating components from external influences becomes uniform, and the temperature gradient is zero-$dh_{1000}/dT = 0$. However, judging by the wear

value, the ion-plasma coating has higher resistance. Lower values of mechanical pressure (1.9 MPa → 6.7 (3.1) MPa) in the friction zone with increasing temperature for the coatings do not predetermine the dynamics of convergence between the coating components, as occurs at higher values. Moreover, the forces of interaction between the components do not increase, the structure does not compact, and the resistance to bond failure does not increase. The coatings are, as it were, ripped apart along the bonds formed during their formation by the application of ring-shaped specimens to the substrate.

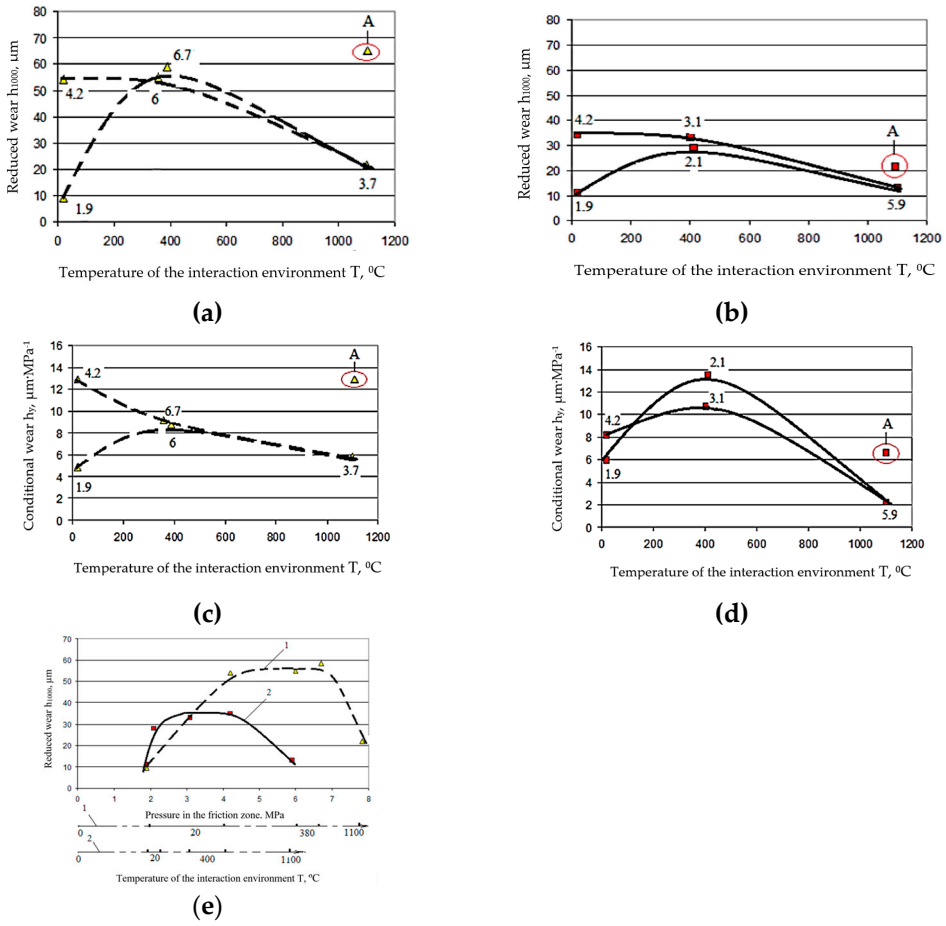

Figure 12. Dependence of coating wear types on interaction temperature: (**a**) reduced linear wear of gas-flame coating; (**b**) reduced linear wear of ion-plasma coating; (**c**) conditional wear of gas-flame coating; (**d**) conditional wear of ion-plasma coating; A—stage 4; (**e**) reduced wear under pressure in the friction zone: 1—gas-flame coating; 2—ion-plasma coating. (The numbers next to the dots indicate the pressure in MPa.).

The gradient of resistance to destruction both by temperature and by force load is the same—positive $dh_{1000}/dT > 0$, $dh_{1000}/dp > 0$. In general, in the temperature range from 20 °C to 400 °C, the leading role in the influence of the mechanical component of interaction on wear processes should be given to the forces of normal and tangential loading of friction contact zones, and their correlation with the forces of interaction between the components of the coatings previously formed by gas-flame and ion-plasma technologies of application to ring samples.

In the temperature range from 400 °C to 1100 °C, both reduced and conventional wear decrease. This decrease occurs for both coatings, regardless of whether the friction zone pressure increases or decreases. This suggests that temperature plays a key role in this case, causing not the compaction of pre-formed structures, but predictable structural and phase transformations within the coatings, fundamentally altering the configuration

of their compositions and bonds [36]. In other words, the structures become secondary, retaining their inherent resistance to mechanical loading. While the average conventional wear values for both coatings in this range are approximately the same, amounting to 6.7 μm MPa^{-1} and occurring at average mechanical pressures of 5.3 MPa (Figure 12c,d), each coating individually exhibits its own unique characteristics. The gas-flame coating is more resistant at a temperature of 400 °C at higher pressures (6.0–6.7 MPa) than the ion-plasma coating at lower pressures (2.1–3.1 MPa). However, at a temperature of 1200 °C, the pattern of resistance to destruction reverses: the gas-flame coating exhibits greater wear at a lower pressure (p = 3.7 MPa) than the ion-plasma coating at a pressure (p = 5.9 MPa). This may be due to the fact that the coatings undergo a change in the wear mechanism, caused by a change in the ratio between the shares of possible plastic and elastic deformations of frictional interaction zones and the ability of microvolumes of structural formations to accumulate fatigue [37]. In this case, based on Figure 12c,d, the strength of cohesive bonds under elastic sliding contact in the ion-plasma coating structure is presumably approximately three times higher than that of the gas-flame coating.

The gas-flame coating is more resistant at a temperature of 400 °C at higher pressures (6.0–6.7 MPa) than the ion-plasma coating at lower pressures (2.1–3.1 MPa). However, at a temperature of 1200 °C, the pattern of resistance to destruction reverses: the gas-flame coating exhibits greater wear at a lower pressure (p = 3.7 MPa) than the ion-plasma coating at a lower pressure (p = 5.9 MPa). This may be due to the fact that the coatings undergo a change in the wear mechanism, caused by a change in the ratio between the shares of possible plastic and elastic deformations of frictional interaction zones and the ability of microvolumes of structural formations to accumulate fatigue [38]. In this case, based on Figure 12c,d, the strength of cohesive bonds under elastic sliding contact in the ion-plasma coating structure is presumably approximately three times higher than that of the gas-flame coating.

By examining the reverse extrapolation of the patterns of change in reduced wear, we can predict the following conclusion. The threshold mechanical pressure for destruction of a flame-oxygen coating may be 1.3–1.35 MPa, while for an ion-plasma coating, this pressure is 1.65–1.7 MPa.

If the surface is damaged to a depth of more than 75–100 μm, both coatings become unusable because their wear resistance (as assessed by linear wear) is no longer maintained. This is evidenced by the rapid decrease in their wear resistance under step loading. Moreover, the gas-flame coating is more prone to catastrophic failure than the ion-plasma coating. A depth of 75–100 μm is considered critical at this stage of research. This follows from the following. The term "critical depth" of wear is formulated based on its value obtained in the fourth stage of modeling after grinding the cutting tracks in the third stage. The thickness of the ground layer was 0.1 mm (100 μm) to cover the maximum depth of 55 μm for the ion-plasma coating (Table 1, experiments No. 1 and No. 2). Then, taking into account the removed layer and wear values of 66.7 ± 26.2 μm and more for the gas-flame coating and 21.3 ± 7.1 μm for the ion-plasma coating, a damage range of more than 75–100 μm was formulated, which is of a presumptive nature.

5. Conclusions

The work involves physical modeling of thermomechanical loading of gas-flame and ion-plasma coatings, simulating the stages of contact between the stator and the gas turbine engine blades. For both types of coatings, a parabolic wear pattern was established with an extreme in the range of 350–450 °C at pressures of 1.9–6.7 MPa.

Wear stabilization is observed only at temperatures of 20–400 °C. For the gas-flame coating, this effect manifests itself at pressures of 4–6.7 MPa, and for the ion-plasma coating,

at 3–4.2 MPa. Ion-plasma coating showed 37% higher wear resistance than gas-flame coating. Under high loads and temperatures (including operating modes up to 1100 °C), it retains better surface geometry, while gas-flame coating is prone to deeper cutting and catastrophic failure.

Gas-flame coating has a "loose" structure with less pronounced wear tracks. Ion-plasma coating has a dense structure, but is prone to forming a wave-like relief, which indicates specific plastic deformation of the surface layers. At a damage depth of more than 75–100 μm, both coatings lose their performance due to a sharp decrease in wear resistance. At the same time, the ion-plasma coating is more prone to the accumulation of fatigue microdeformations, while the gas-flame coating is more prone to mechanical destruction.

Further research will focus on modeling wear in the critical temperature range (1100–1200 °C), where the properties of the coatings under consideration begin to equalize.

Author Contributions: Conceptualization, V.K. (Vadim Kubich), A.I. and O.C.; methodology, V.K. (Vitaliy Kulikov), S.K., and Y.F.; software, Y.F., O.Z., S.A. and O.C.; validation, V.K. (Vadim Kubich), O.Z., S.K. and A.I.; formal analysis, V.K. (Vitaliy Kulikov); investigation, V.K. (Vadim Kubich) and A.I.; resources, O.Z., S.A., S.K., Y.F., O.C., and A.I.; data curation, O.C.; writing—original draft preparation, V.K. (Vadim Kubich), O.Z. and V.K. (Vitaliy Kulikov); writing—review and editing, S.K., S.A.; visualization, V.K. (Vadim Kubich), O.Z.; supervision, V.K. (Vadim Kubich); project administration, V.K. (Vadim Kubich), S.K. and O.Z.; funding acquisition, V.K. (Vitaliy Kulikov). All authors have read and agreed to the published version of the manuscript.

Funding: This research was conducted as part of grant AP 26199877 from the Science Committee of the Ministry of Education and Science of the Republic of Kazakhstan, entitled "Development of technology for applying composite protective coatings to equipment parts in the metallurgical and machine-building industries".

Data Availability Statement: The raw data supporting the conclusions of this article will be made available by the authors on request. Data is available from the corresponding author upon reasonable request.

Conflicts of Interest: The authors declare no conflicts of interest.

References

1. Ułanowicz, L.; Dudzi'nski, A. Heat-Resistant Protective Coatings Applied to Aircraft Turbine Blades by Supersonic Thermal Spraying and Diffusion-Aluminizing. *Coatings* **2024**, *14*, 1554. [CrossRef]
2. Brodzik, Ł. Gas Temperature Distribution in the Combustion Chamber of a GTM400 MOD Turbojet Engine Powered by JET A-1 Fuel and Hydrogen. *Energies* **2024**, *17*, 745. [CrossRef]
3. Ułanowicz, L.; Dudzi'nski, A. Two-Layer Heat-Resistant Protective Coatings for Turbine Engine Blades. *Coatings* **2023**, *13*, 588. [CrossRef]
4. Zhang, B.; Li, J.; Li, W.; Ji, H. Influence of Geometric Tooth Shape Parameters of Labyrinth Seals on the Flow Law and the Algorithm for Designing Straight Grate Teeth. *Russ. Phys. J.* **2021**, *64*, 1122–1129. [CrossRef]
5. Enache, M.; Carlanescu, R.; Mangra, A.; Florean, F.; Kuncser, R. Investigation of Flow through a Labyrinth Seal. *Incas Bull.* **2021**, *13*, 51–58. [CrossRef]
6. Gurrola Arrieta, M.d.J.; Botez, R.M.; Lasne, A. An Engine Deterioration Model for Predicting Fuel Consumption Impact in a Regional Aircraft. *Aerospace* **2024**, *11*, 426. [CrossRef]
7. Osorio, J.D.; Toro, A.; Hernández-Ortiz, J.P. Hernández-Ortiz Thermal Barrier Coatings for Gas Turbine Applications: Failure Mechanisms and Key Microstructural Features. *Dyna* **2012**, *79*, 149–158.
8. Mangra, A.; Florean, F.; Radu, A. Analytical and numerical investigation of flow through a labyrinth seal. *UPB Sci. Bull. Ser. D Mech. Eng.* **2021**, *83*, 169–180.
9. Yu, B.; Ke, H.; Shen, E.; Zhang, T. A review of blade tip clearance–measuring technologies for gas turbine engines. *Meas. Control* **2020**, *53*, 339–357. [CrossRef]
10. Čížek, M.; Pátek, Z. On CFD Investigation of Radial Clearance of Labyrinth Seals of a Turbine Engine. *Acta Polytech.* **2020**, *60*, 38–48. [CrossRef]

11. Borysov, Y.S.; Vihilianska, N.V.; Burlachenko, O.M.; Olevska, L.P.; Lopata, V.M. Analysis of modern experience in development of sealing coatings for parts of gas turbine engines. *Paton Weld. J.* **2022**, *4*, 34–42. [CrossRef]
12. Ullah, A.; Khan, A.; Bao, Z.B.; Yang, Y.F.; Xu, M.M.; Zhu, S.L.; Wang, F.H. Temperature Effect on Early Oxidation Behavior of NiCoCrAlY Coatings: Microstructure and Phase Transformation. *Acta Metall. Sin.* **2021**, *35*, 975–984. [CrossRef]
13. Yang, H.; Wu, Y.; Sun, Q.; Yang, F.; Xia, C.; Xia, S.; Du, J. Study on High Temperature Properties of Yttrium-Modified Aluminide Coating on K444 Alloy by Chemical Vapor Deposition. *Coatings* **2024**, *14*, 750. [CrossRef]
14. Jojith, R.; Sam, M.; Radhika, N. Recent advances in tribological behavior of functionally graded composites: A review. *Eng. Sci. Technol. Int. J.* **2021**, *25*, 100999. [CrossRef]
15. Li, M.; Xie, J.; Gao, W.; Zhan, Z.; Li, Z. Effect of yttrium on the oxidation resistance and areaspecific resistance of $MnCo_2O_4$ coating. *Surf. Coat. Technol.* **2022**, *444*, 128655. [CrossRef]
16. Yefanov, V.; Ovchynnykov, O.; Dzhuhan, O.; Raspornia, D.; Saprykin, Y. Developing themodification of nickel cathodes for applying the ion-plasma coatings on the parts of aircraf engines. *East.-Eur. J. Enterp. Technol.* **2020**, *4*, 6–13.
17. Bansal, U.; Esakkiraja, N.; Baskaran, T.; Paul, T.; Ravi, R.; Kumar, P.; Jayaram, V.; Paul, A. Synergistic effects of Pt and Y addition in (Ni, Pt)CrAlY bond coat on oxide spallation resistance and growth of interdiffusion zone between bond coat and Ni-based single crystal superalloy. *Corros. Sci.* **2024**, *240*, 112485. [CrossRef]
18. Liu, Y.; Huang, C.; Yang, H.; Sun, X.; Zhang, H.; Sun, Y.; Zhang, W.; Lan, H.; Yu, S. Enhanced Corrosion Resistance of CuAl/BN Coatings through the Addition of Rare Earth Elements and High-Temperature Oxidation Treatment. *Crystals* **2024**, *14*, 808. [CrossRef]
19. Wu, Y.; Li, Y.; Xu, Y.; Kang, M.; Wang, J.; Sun, B. Unveiling the mechanism of yttrium-related microstructure inhibiting or promoting high-temperature oxidation based on Ni-Al-Y alloys. *Acta Mater.* **2021**, *211*, 116879. [CrossRef]
20. Bertuol, K.; Arendarchuck, B.E.; Stoyanov, P. An Overview of Metallic Abradable Coatings in Gas Turbine Engines. *Coatings* **2025**, *15*, 1216. [CrossRef]
21. Ching, H.A.; Choudhury, D.; Nine, M.J.; Osman, N.A. Effects of surface coating on reducing friction and wear of orthopaedic implants. *Sci. Technol. Adv. Mater.* **2014**, *15*, 014402. [CrossRef]
22. Zhetessova, G.; Zharkevich, O.; Pleshakova, Y.; Yurchenko, V.Y.; Platonova, Y.; Buzauova, T. Building mathematical model for gasthermal process of coating evaporation. *Metalurgija* **2016**, *55*, 63–66.
23. Pakhomova, E.; Palombi, A.; Varone, A. Plasma Spraying of W Coatings for Nuclear Fusion Applications: Advancements and Challenges. *Crystals* **2025**, *15*, 408. [CrossRef]
24. Czupryński, A.; Mele, C. Properties of flame spraying coatings reinforced with particles of carbon nanotubes. *Adv. Mater. Sci.* **2021**, *21*, 57–76. [CrossRef]
25. Kubich, V.; Fasol, Y.; Cherneta, O.; Yershina, A.K.; Sakipov, N.Z. Resistance of heat-resistant yttrium-containing sealing coatings to mechanical fracture when forming cutting paths. *Eurasian Phys. Tech. J.* **2024**, *21*, 81–92. [CrossRef]
26. Fasol, Y.O.; Kubich, V.I.; Cherneta, O.G.; Yurov, V.M.; Rabatuly, M. Evaluation of Wear of Gas-Flame and Ion-Plasma Sealing Coatings with 0.3% Yttrium under Thermomechanical Loading Conditions. *Mater. Mech. Eng. Technol.* **2025**, 10–15. [CrossRef]
27. Kubich, V.; Fasol, E.; Cherneta, O. Influence of high-temperature loading conditions on the change in the physical state of yttrium-containing coatings. *Probl. Frict. Wear* **2024**, *102*, 14–22. [CrossRef]
28. Kubich, V.; Fasol, Y. Defining tests of heat-resistant yttrium-containing sealing coatings for high-temperature gas-erosion resistance. *Probl. Frict. Wear* **2023**, *100*, 40–48. [CrossRef]
29. *EN ISO 4782:1987*; Industrial Wire Screens and Woven Wire Cloth — Diameters of Metal Wire. International Organization for Standardization (ISO): Geneva, Switzerland, 1987.
30. *ISO 3310-1:2017*; Test Sieves — Technical Requirements and Testing — Part 1: Test Sieves of Metal Wire Cloth. ISO (International Organization for Standardization): Geneva, Switzerland, 2016.
31. *GOST 5632-2014*; Alloyed Stainless Steels and Alloys: Corrosion-Resistant, Heat-Resistant, and Temperature-Resistant (Minsk, CIS Countries). Federal Agency on Technical Regulating and Metrology (Rosstandart): Moscow, Russia, 2014.
32. Alqallaf, J.; Ali, N.; Teixeira, J.A.; Addali, A. Solid Particle Erosion Behaviour and Protective Coatings for Gas Turbine Compressor Blades—A Review. *Processes* **2020**, *8*, 984. [CrossRef]
33. Roth, J.R. *Industrial Plasma Engineering*, 1st ed.; Volume 1: Principles; CRC Press: Boca Raton, FL, USA, 2025; Volume 1, p. 235.
34. Turbin, P.V.; Beresnev, V.M.; Horokh, D.V. Properties Evolution of Ion-plasma Coatings on the Base of Transition Metal Nitrides. *J. Nano-Electron. Phys.* **2020**, *12*, 05031. [CrossRef] [PubMed]
35. Kudryakov, O.; Kolesnikov, V.; Varavka, V.; Polityko, K. Optimization of the Ion-Plasma Tribological Coatings Properties by a Desirability Function Constructing. In *Proceedings of the 11th International Conference on Industrial Engineering, Sochi, Russia, 11–27 May 2025*; Springer Nature: Cham, Switzerland, 2025; pp. 534–543. [CrossRef]
36. Chabak, Y.G.; Efremenko, V.G.; Zurnadzhy, V.I.; Efremenko, B.V.; Petryshynets, I. *Improvement of Wear Resistance of Steels and Cast Irons by Pulsed-Plasmasurface Modification and Coating Deposition*; Premier Publishing: Prague, Czech Republic, 2024; p. 172.

37. Holmberg, K.; Matthews, A. *Coatings Tribology Properties, Mechanisms, Techniques and Applications in Surface Engineering*; Elsevier: Amsterdam, The Netherlands, 2009; p. 560.
38. Babak, V.P.; Bilchuk, Y.Y.; Shchepetov, V.V. Increased Wear Coatings due Intrastructural Self-Correction. *J. Eng. Sci.* **2019**, *6*, 11–15. [CrossRef]